

# First-Principles Study of the Band Gap Structure of Oxygen-Passivated Silicon Nanonets

Linhan Lin · DeXing Li · Jiayou Feng

Received: 2 November 2008 / Accepted: 19 January 2009 / Published online: 6 February 2009  
© to the authors 2009

**Abstract** A net-like nanostructure of silicon named silicon nanonet was designed and oxygen atoms were used to passivate the dangling bonds. First-principles calculation based on density functional theory with the generalized gradient approximation (GGA) were carried out to investigate the energy band gap structure of this special structure. The calculation results show that the indirect-direct band gap transition occurs when the nanonets are properly designed. This band gap transition is dominated by the passivation bonds, porosities as well as pore array distributions. It is also proved that Si–O–Si is an effective passivation bond which can change the band gap structure of the nanonets. These results provide another way to achieve a practical silicon-based light source.

**Keywords** Silicon nanonets · Oxygen-passivated · First-principles calculation · Direct band gap · Porosity · Pore array distribution

## Introduction

Being the basic material of modern integrated circuit technology for decades, silicon is one of the most important semiconductor materials. Due to its indirect band gap structure, the applications of silicon in optoelectronics are still limited. Nowadays, semiconductors with nanoscale structures are of great interest. It is believed that silicon

will develop a direct band gap in nanoscale structures. A number of attempts such as porous silicon [1–3], silicon nanocrystals [4, 5], and silicon nanowires [6, 7] have been carried out to eliminate the obstacle. Other attempts such as Si/SiO<sub>2</sub> superlattices structure [8, 9], Si/Ge quantum cascade [10], erbium-doped silicon-rich silicon oxide [11, 12], and all-silicon Raman laser [13] are also employed to achieve this luminescent transition. However, the practical silicon-based light source is still out of reach. A new silicon-based structure which is named silicon nanonet is presented in our study. It is a net-like structure constructed by drilling nanopore arrays along a special direction. The depths of the pores are of macroscale while the pore diameters and the pore walls are of nanoscale. It is found that the band structure of the nanonets changes from indirect to direct band gap when proper designs are provided.

## Calculation Details

Four types of nanopore array distributions are discussed here, as shown in Fig. 1. The pore sides of the nanonets have numbers of dangling bonds. Thus, Si–O–Si, Si–OH, as well as Si–H are selected as passivation bonds. Hydrogen atoms are usually used for passivation in constructing models of nanoscale. However, it is known that Si–H bond is of poor stabilization in the air. It will be replaced by Si–O bond, which is a stable state on the silicon surface. Si–O passivation is also easy to achieve by exposing the sample in the air [14, 15], electrochemical oxidation [16], or thermal oxidation [17] and has already been introduced into the microelectronics devices. It has also been widely studied in order to improve the luminescence property of porous silicon [18]. For the 100 nanonets, most of the

L. Lin · D. Li · J. Feng (✉)  
Department of Materials Science and Engineering, Key Lab of Advanced Materials, Tsinghua University, Beijing 100084, China  
e-mail: fengjy@mail.tsinghua.edu.cn

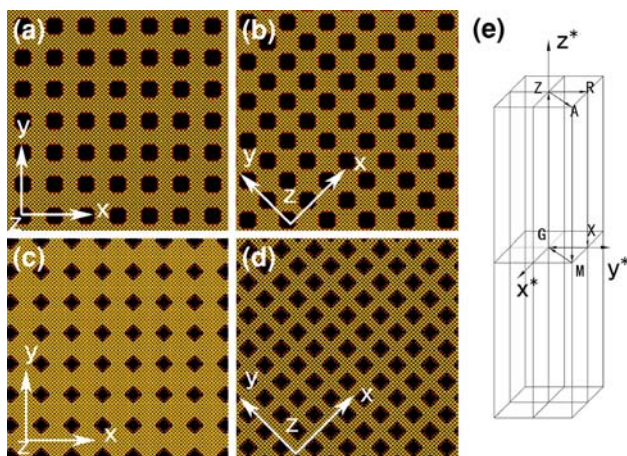


**Fig. 1** Schematic view of **a** 100X4B5W3P29O, **b** 100D5B5W2P29O, **c** 110D4B6W2P20OH, **d** 110X4B6W2P20OH, and **e** special points in the reciprocal space of nanonets. For (a)–(d), 100 or 110 represents the orientations of the pore sides, Xi or Di depends on the shapes and the sizes of the primitive cell of the silicon nanonets, Bj indicates the bore diameters of the nanopore, Wk is the minimal widths of the nanowall, Pn means the porosities of the silicon nanonets. OH means the nanowalls are OH-passivated, while O indicates the nanowalls are passivated by Si–O–Si. The crystal orientations of the primitive cells of the 100D and 110X nanonets have a 45° rotation compared with the other two models: the *x* and *y*-axis of 100X and 110D are [100], while [110] for 110X and 110D

silicon atoms on the pore walls have two dangling bonds. We use oxygen-bridge to link neighboring silicon atoms in sides and hydrogen atoms to passivate silicon atoms in corners (Fig. 1a, b). For the 110 models, each silicon atom on the pore walls has only one dangling bond. Therefore, hydroxyl is used for passivation and the Si atoms in the corners are also passivated by H in order to reduce the internal stress (Fig. 1c, d). The special points in the reciprocal space of the nanonets and the paths in our calculation are shown in Fig. 1e. The coordinate axes in the reciprocal space are established corresponding to the axes of the real space shown in Fig. 1a–d.

The calculations of energy band structure of the silicon nanonets were based on the local density approximation and density function theory (LDA–DFT). The generalized gradient approximation (GGA), for the exchange and correlation effects [19] with the ultrasoft pseudopotentials [20] was selected for the calculations. These pseudopotentials require a quite low energy cut-off and guarantee good transferability and robustness. A geometry optimization of the silicon nanonets was carried out first with the atomic positions and the crystal cell parameters relaxed by total energy minimization. For the calculations of electronic characteristic, the cut-off energy of 340 eV was assumed in the plane-wave basis set, the SCF convergence tolerance of the electronic energy per atom was  $1 \times 10^{-6}$  eV and the *k*-point separation was  $0.4 \text{ nm}^{-1}$ .

## Results and Discussion

After the geometry optimization of the silicon nanonets, the atomic positions and the cell parameters become reasonable. The bond lengths are similar to the results reported in the study of siloxenic clusters [21]. As the length of Si–O bond is much smaller than the Si–Si bond, the distance between the silicon atoms which are linked by the same oxygen atom becomes much smaller in the Si–O–Si passivated nanonets. Hence, the presence of the oxygen atoms on the nanowalls of the Si–O–Si passivated nanonets produces a local diminution of the second-neighbor separation for silicon lattice, and consequently a structural contraction. For the –OH-passivated nanonet models, the Si–Si bond length increases in the case that both of the silicon atoms are linked with –OH, and decreases in the case that one silicon atom is linked with hydroxyl while the other with hydrogen. This is due to the different interactions between the passivation atoms.

Figure 2 shows the band structures of Si and some nanonets constructed with  $4 \times 4 \times 1$  supercell. Si exhibits a typical indirect band gap. However, when the nanopore arrays are introduced in the silicon supercell, both the conduction band and the valence band are significantly changed. The direct band gap structure appears in the nanonets with special parameters.

In Fig. 2a, it is shown that the conduction band minimum (CBM) of bulk Si moves to 1/3 GZ or X due to the folding effect, which is in accordance with the theoretical analysis. In the 100X nanonets, the notable changes of the valence band occur at X. For the bulk Si, a valley exists at point X, which is much lower than G. With the porosity increases, the value of X increases and the valley disappears when the porosity reaches 29%. The G–X are 0.26, 0.08, 0.06, and 0.04 eV for bulk Si, 100X4B4W4P16O, 100X3B4W2P29O and 100X4B6W2P45O, respectively. However, G is always the valence band maximum (VBM) in all the 100X nanonets we concerned, which is the same with the location of VBM in bulk Si. In the conduction band, the changes of X are most important. With the porosity increases, the X–G changes from negative to positive and the CBM moves from X to G, leading to an indirect to direct band gap transition. All the 100X nanonets with porosities higher than 29% exhibit direct band gap structure in our calculation (Fig. 2c, d). For the 100D nanonets, it should be noted that the coordinate axes have been rotated a degree of 45° compared with the 100X nanonets. Thereby, the paths of ZAMGZRXC shown in the band structure of 100D nanonets correspond to ZRXG–ZAMG in the 100X nanonets. The location of CBM is fixed at M and the change of the M–G in the valence band is the key factor of the band gap transition. Our results show that the values of M–G are negative for 100D3B4W2P25O and

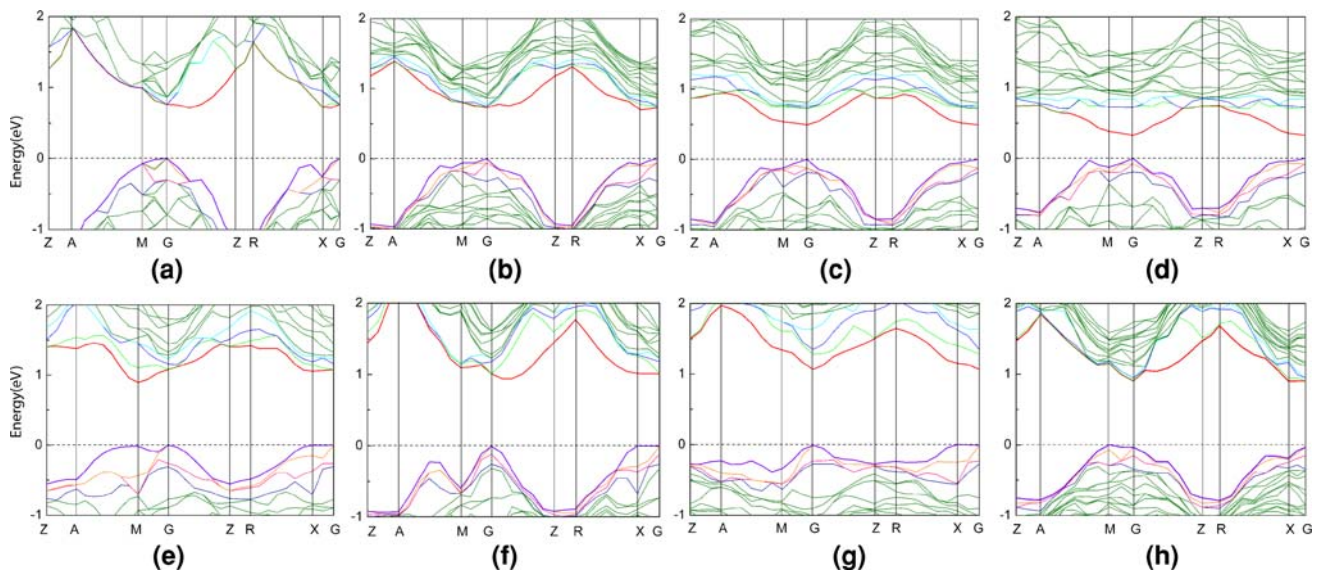


**Fig. 2** Energy band gap structure of Bulk silicon and nanonets with the same cell size:  $4 \times 4 \times 1$  supercell. **a** Bulk Si (VBM: G, CBM: 1/3GZ, Eg: 0.71 eV), **b** 100XB4W4P16O (VBM: G, CBM: X, Eg: 0.74 eV), **c** 100X4B5W3P29O (VBM: G, CBM: G, Eg: 0.49 eV), **d** 100X4B6W2P45O (VBM: G, CBM: G, Eg: 0.32 eV), **e** 100D4B4W2P33O

(VBM: G, CBM: M, Eg: 0.90 eV), **f** 110X4B4W4P14OH (VBM: X, CBM: 1/6 GZ or 1/3 GZ, Eg: 0.94 eV), **g** 110X4B6W2P39OH (VBM: X, CBM: G, Eg: 1.07 eV), **h** 110D4B6W2P20OH (VBM: M, CBM: X, Eg: 0.90 eV)

100D4B4W2P33O (Fig. 2e). However, when the porosity reaches 37%, the G–M becomes positive and the VBM moves from G to M and result in a direct band gap. Both the Si–O–Si passivated 100X and 100D nanonets exhibit the band gap transitions when the porosities are increased. However, the location of the VBM and CBM are different for these two models when direct band gap is obtained. Both the VBM and CBM locate at G for the 100X nanonets, while M for the 100D nanonets. This indicates that the distribution of the nanopore arrays is another key factor of the band gap structure of nanonets.

The 110X nanonets have the same macro appearance compared with the 100X nanonets, only with the difference of the crystal orientation of Si substrate. It should also be noted that a  $45^\circ$  rotation exists between the coordinate axes of the 110X nanonets and the 100X nanonets, which lead to the difference of the special points shown in the band structure. The motion of CBM appears in the GZ path. When the porosity is lower than 30%, the CBM stays at 1/6 GZ or 1/3 GZ (Fig. 2f). However, when the porosity increases to 39%, the CBM move from 1/6 GZ or 1/3 GZ to G (Fig. 2g). As the VBM always stays at X, the 110X nanonets exhibit indirect band gap in various porosities we study. The 110D nanonets can be treated as the 100X nanonets with the pore side orientation rotates a degree of  $45^\circ$ . Similar to the 110X nanonets, the 110D nanonets with different porosities in our study present indirect band gap with the CBM at point X and the VBM at point M

(Fig. 2h). Both the –OH-passivated 110X and 110D nanonets have indirect band gap in different porosities, which is rather different from the results of 100X and 100D Si–O–Si passivated nanonets.

The pore wall width is the key factor in deciding the band gap of the nanonets. With the decreases of the pore wall width, the band gap increases due to the quantum confinement effect caused by the nanoscale of the pore walls. It should be noticed that the underestimation of the band gap induced by the approximation in the electron exchange-correlation energy in LDA–DFT method exists in this study without any correction.

It is shown that nanonets with the nanopore array distributions of 100X and 100D exhibit direct band gap characteristic when the porosity exceeds a special value. However, the passivation bonds can also lead to the changes of the band gap structure. In order to confirm our arguments, the band gap structure of 100D nanonets with different passivation conditions is studied here. The CBM of 100D5B5W2P37H, all the dangling bonds on the nanowalls of which are passivated by –H, stays at point G. However, the XG path in the valence band is almost horizontal, which indicates that the electrons on the corresponding state act as a two-dimensional electron gas in the real space (Fig. 3a). When the passivation bonds are taken place by Si–O–Si, both the VBM and the CBM move to M and result in a direct band gap (Fig. 3b). The value of the band gap is also reduced due to the Si–O–Si passivation

**Fig. 3** Band gap structure of **a** 100D5B5W2P37H (VBM: X or G, CBM: G, Eg: 1.28 eV), **b** 100D5B5W2P37O (VBM: M, CBM: M, Eg: 0.59 eV)

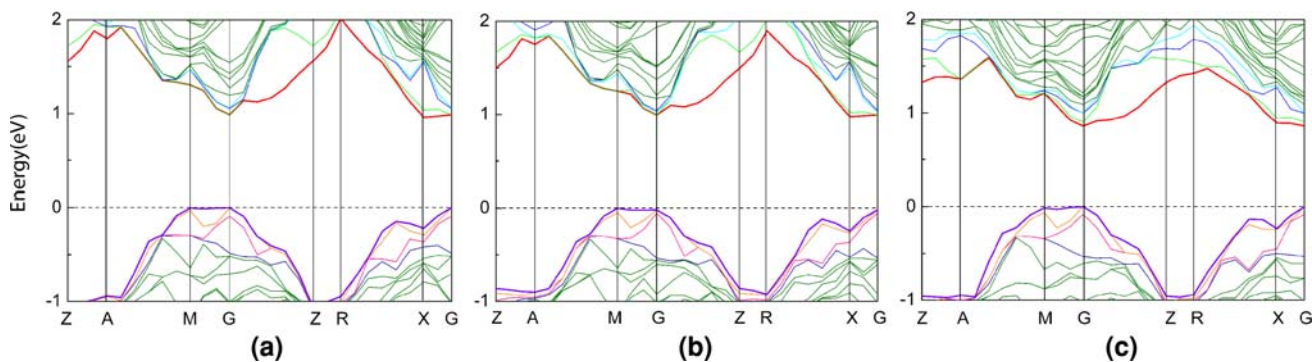
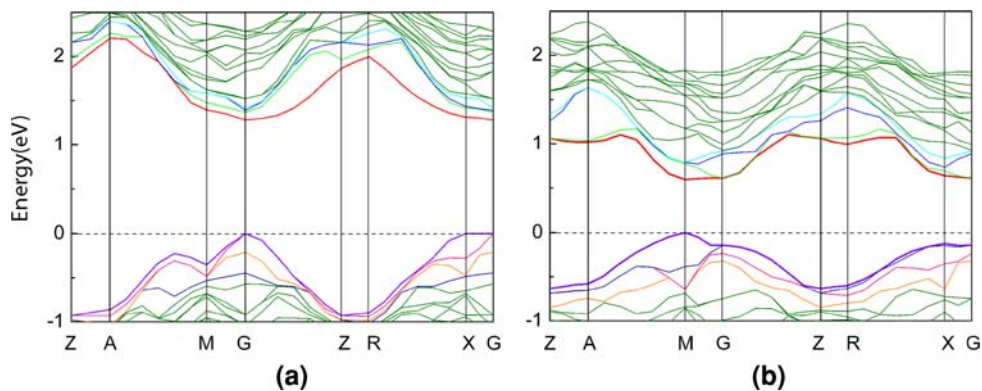


**Fig. 4** Band gap structure of silicon nanonets with the same parameters but different passivation conditions **a** 110D3B4W2P13H (VBM: M or G, CBM: X, Eg: 0.96 eV), **b** 110D3B4W2P13OH (VBM: M, CBM: X, Eg: 0.98 eV), **c** 110D3B4W2P13O (VBM: G, CBM: G, Eg: 0.86 eV)

bonds. For further study of the effect of the different passivation bonds, the band structures of 110D nanonets with the same nanopore structure but passivated by  $-H$ ,  $-OH$ , and  $Si-O-Si$ , respectively, were calculated here. As shown in Fig. 4, 110D3B4W2P13H has an indirect band gap with the VBM at M and CBM at X, which is almost the same with 110D3B4W2P13OH. However, when the passivation bonds are taken place by  $Si-O-Si$ , both the CBM and VBM move to point G and a direct band gap structure is obtained. This indicates that  $Si-O-Si$  bond is an effective passivation bond which has greater influence on the band edge of nanonets, compared with the H and OH-passivated nanonets. It is due to the contribution of the electrons on the  $O-2p$  orbits in the  $Si-O-Si$  bond. The density of states (DOS) near the band edge of nanonets contributed by the oxygen atoms in  $Si-O-Si$  is larger than that of the hydrogen atoms in  $Si-H$  and the oxygen atoms in  $Si-OH$ . It is noted that the change of the band gap structure is not as obvious as that of the 110D nanonets shown in Fig. 3. This is because the number of the  $Si-O-Si$  bonds in the 110D3B4W2P13O is limited. In addition, the band gap is found to be in conjunction with the passivation bonds. The band gaps of 110D3B4W2P13H and 110D3B4W2P13OH are almost the same, 0.96 and 0.98 eV, respectively. However, it

decreases to 0.86 eV for 110D3B4W2P13O, which may lead to the red shift in the photoluminescence spectrum.

## Conclusions

In summary, the structure design of oxygen-passivated silicon nanonets could result in indirect–direct band gap transitions of silicon. The  $Si-O-Si$  passivated 100X and 100D nanonets exhibit direct band gap characteristic when the porosities exceed 29 and 37%, respectively. The  $-OH$ -passivated 110D and 110X nanonets with different porosities we concerned in this study have indirect band gap.  $Si-O-Si$  bond has more effective influence on the band edge region of the nanonets than  $-H$  or  $-OH$  bonds and is expected to change the band gap structure of silicon nanonets. With the rapid development of the materials nano fabrication, it is expected that this electronic characteristic of the nanonets could be validated in experiments.

**Acknowledgments** This work was supported by National Natural Science Foundation of China (Grant No. 50571050), the National Basic Research Program of China (973 program, Grant No. 2007CB936601) and Tsinghua National Laboratory for Information Science and Technology of China.

## References

1. L.T. Canham, *Appl. Phys. Lett.* **57**, 1046 (1990). doi:[10.1063/1.103561](https://doi.org/10.1063/1.103561)
2. L.T. Canham, W.Y. Leong, M.I.J. Beale, T.I. Cox, L. Taylor, *Appl. Phys. Lett.* **61**, 2563 (1992). doi:[10.1063/1.108127](https://doi.org/10.1063/1.108127)
3. A. Halimaoui, C. Oules, G. Bomchil, *Appl. Phys. Lett.* **59**, 304 (1991). doi:[10.1063/1.105578](https://doi.org/10.1063/1.105578)
4. P. Mutti, G. Ghislotti, S. Bertoni, L. Bonoldi, *Appl. Phys. Lett.* **66**, 851 (1995). doi:[10.1063/1.113408](https://doi.org/10.1063/1.113408)
5. N.A. Hill, K.B. Whaley, *Phys. Rev. Lett.* **75**, 1130 (1995). doi:[10.1103/PhysRevLett.75.1130](https://doi.org/10.1103/PhysRevLett.75.1130)
6. T.K. Sham, S.J. Naftar, P.-S.G. Kim, R. Sammynaiken, Y.H. Tang, *Phys. Rev. B* **70**, 45313 (2004). doi:[10.1103/PhysRevB.70.045313](https://doi.org/10.1103/PhysRevB.70.045313)
7. L. Brus, *J. Phys. Chem.* **98**, 3575 (1994). doi:[10.1021/j100065a007](https://doi.org/10.1021/j100065a007)
8. B.T. Sullivan, D.J. Lockwood, H.J. Labbé, Z.-H. Lu, *Appl. Phys. Lett.* **69**, 3149 (1996). doi:[10.1063/1.116811](https://doi.org/10.1063/1.116811)
9. Z.H. Lu, D.J. Lockwood, J.-M. Baribeau, *Nature* **378**, 258 (1995). doi:[10.1038/378258a0](https://doi.org/10.1038/378258a0)
10. L. Diehl, S. Mentese, E. Müller, D. Grützmacher, H. Sigg, *Appl. Phys. Lett.* **81**, 4700 (2002). doi:[10.1063/1.1528729](https://doi.org/10.1063/1.1528729)
11. H.S. Han, S.Y. Seo, J.H. Shin, *J. Appl. Phys.* **88**, 2160 (2000). doi:[10.1063/1.1304838](https://doi.org/10.1063/1.1304838)
12. J.H. Shin, S.Y. Seo, *Appl. Phys. Lett.* **76**, 1999 (2000). doi:[10.1063/1.126234](https://doi.org/10.1063/1.126234)
13. H. Rong, A. Liu, R. Jones, O. Cohen, *Nature* **433**, 292 (2005). doi:[10.1038/nature03273](https://doi.org/10.1038/nature03273)
14. Y.H. Ogata, T. Tsuboi, T. Sakka, S. Naito, *J. Porous Mater.* **7**, 63 (2000). doi:[10.1023/A:1009694608199](https://doi.org/10.1023/A:1009694608199)
15. G. Mattei, V. Valentini, V.A. Yakovlev, *Surf. Sci.* **2002**(502), 58 (2002). doi:[10.1016/S0039-6028\(01\)01898-2](https://doi.org/10.1016/S0039-6028(01)01898-2)
16. R. Boukherroub, D.D.M. Wayner, D.J. Lockwood, *Appl. Phys. Lett.* **81**, 601 (2002). doi:[10.1063/1.1492306](https://doi.org/10.1063/1.1492306)
17. J. Salonen, V.P. Lehot, E. Laine, *Appl. Phys. Lett.* **70**, 637 (1997). doi:[10.1063/1.118294](https://doi.org/10.1063/1.118294)
18. B. Geloz, A. Kojima, N. Koshida, *Appl. Phys. Lett.* **87**, 031107 (2005). doi:[10.1063/1.2001136](https://doi.org/10.1063/1.2001136)
19. J.P. Perdew, J.A. Chevary, S.H. Vosko, K.A. Jackson, *Phys. Rev. B* **46**, 6671 (1992). doi:[10.1103/PhysRevB.46.6671](https://doi.org/10.1103/PhysRevB.46.6671)
20. D. Vanderbilt, *Phys. Rev. B* **41**, 7892 (1990). doi:[10.1103/PhysRevB.41.7892](https://doi.org/10.1103/PhysRevB.41.7892)
21. M.R. Pederson, W.E. Pickett, *Phys. Rev. B* **48**, 17400 (1993)